Circular Airy beams realized via the photopatterning of liquid crystals [Invited]

Yuan Zhang (张 媛)[1,†], Bingyan Wei (魏冰妍)[1,†,*], Sheng Liu (刘 圣)[1], Peng Li (李 鹏)[1], Xin Chen (陈 馨)[1], Yunlong Wu (吴云龙)[2], Xian'an Dou (豆贤安)[2], and Jianlin Zhao (赵建林)[1,]**

[1]MOE Key Laboratory of Material Physics and Chemistry under Extraordinary Conditions, and Shaanxi Key Laboratory of Optical Information Technology, School of Physical Science and Technology, Northwestern Polytechnical University, Xi'an 710129, China

[2]State Key Laboratory of Pulsed Power Laser Technology, National University of Defense Technology, Hefei 230037, China

**Corresponding author: wbyxz@nwpu.edu.cn; **corresponding author: jlzhao@nwpu.edu.cn*

Received June 20, 2020; accepted July 17, 2020; posted online August 4, 2020

The generation of an autofocusing circular Airy beam (CAB) is realized via a liquid crystal (LC) geometric phase plate with a simple configuration. The fabrication of the LC plate is based on the photoalignment technology and dynamic exposure skill. A focal length of 74 cm is obtained, and the propagation dynamics are consistent with the simulations. Besides, a defocusing CAB is also generated, and the switch between the autofocusing and defocusing CABs can be achieved by controlling the input polarization state. This work provides a convenient and flexible approach to acquire CABs, which will promote the CAB-related applications and researches.

Keywords: circular Airy beam; autofocusing; liquid crystal; photoalignment technique.
doi: 10.3788/COL202018.080008.

An Airy beam is a propagation-invariant wave travelling along a curved parabolic trajectory while being resilient to perturbations. In other words, the Airy beam features non-diffraction, transverse acceleration, and self-healing characteristics. An ideal Airy beam consists of a main lobe and a series of adjacent side lobes trailing off to infinity whose intensity distribution follows the Airy function. These remarkable properties endow Airy beams with numerous attention, especially since their first experimental demonstration was realized by Siviloglou *et al.* via introducing an exponential truncation aperture[1]. Both the one- and two-dimensional Airy wave packets were derived from the Schrödinger equation in a Cartesian coordinate system. Afterwards, circular Airy beams (CABs) were proposed[2] and realized[3] based on cylindrical coordinates. The intrinsic lateral acceleration of the Airy beams during the diffraction-free propagation results in the peculiar autofocusing property of the CAB[2]. Namely, the CABs will keep a relatively low intensity before abrupt autofocusing with peak intensity increased by orders of magnitude. This feature is crucial for situations where high-energy lasers are needed inside transparent objects while the samples before the focus are required to be intact. Therefore, CABs show unique advantages in laser ablation and biomedical treatments like laser nanosurgery[3]. In addition, CABs have also been applied in microparticles' manipulation[4] and the generation of nonlinear intense light bullets[5]. Moreover, they are excellent candidates for igniting nonlinear processes[6] such as optical filaments in gases, stimulated Raman scattering, multiphoton absorption, and so on.

The main strategy for generating CABs is based on the Fourier transform (FT) technique[3,7,8], i.e., modulating a Gaussian beam through the FT pattern of a CAB and then adopting a lens to perform the FT. Another way is utilizing holograms calculated by computing the interference of CABs and the plane wave[4,9]. Usually a $4f$ system consisting of two lenses is demanded to filter the desired orders. For the design of the Fourier mask, a simpler and more convenient method is the superimposition of specific phase distributions[10]. In most of the above approaches, spatial light modulators (SLMs) are employed to display the phase patterns. However, the efficiency and quality of the output CABs are typically limited by the complex electrode matrices of the SLMs[11]. Besides, there must be beam expanders to match the size of the SLM chips, leading to a longer working distance and higher cost for the SLM-based optical systems.

To overcome the shortcomings mentioned above, we propose a liquid crystal (LC) geometric phase plate, LC circular Airy plate (CAP), to generate CABs. The LC-mediated geometric phase optical elements are remarkable candidates for efficient manipulation of light waves[12–18]. On the basis of the phase superimposition strategy, we fabricate the LC CAP via the sulfonic azo-dye SD1-based photoalignment technology and the digital micro-mirror device (DMD)-based micro-lithography system[19]. The obtained CAB autofocuses following a parabolic trajectory at a distance of 74 cm, which matches well with the simulations. In addition to the autofocusing property, defocusing can also be achieved by changing the helicity of the incident circularly polarized light, showing the

polarization-controllable autofocusing/defocusing property. These tunabilities will enrich CABs' applications in optics, photonics, and even interdisciplinary areas.

Based on asymptotic analysis, the FT of a CAB is proportional to the zero-order Bessel function[7], whose argument contains a linear term and a cubic term. Therefore, the phase pattern for the CAB's generation can be simply configured by superimposing the radial linear phase and the radial cubic phase, that is,

$$\varphi = 2\pi r/d + \beta r^3, \tag{1}$$

where $r = \sqrt{x^2 + y^2}$, d is the linear period, and β is a parameter relating to the cubic phase modulation. Figure 1(a) shows a radial linear phase pattern with a period of 70 pixels (1080 pixels in total in the x or y direction), and Fig. 1(b) shows a radial cubic phase pattern with a modulation range of -8π to 8π. Figure 1(c) is the sum of the former two. In order to improve the efficiency of phase modulation, we additionally introduce the geometric phase, which describes the relationship between the phase change and the polarization conversion[18]. Herein, we set the orientation following $\alpha = \varphi/2$. Therefore, Fig. 1(c) could also be regarded as the optical axis distribution with black to white corresponding to the optical axis varying from 0 to π.

To carry out the above design, we take nematic LC E7 as the anisotropic medium and adopt sulfonic azo-dye SD1 as the alignment material. The SD1 molecules are sensitive to UV light and will orientate perpendicularly to the incident polarization direction. The orientation of SD1 will be further spread to the adjacent LCs by intermolecular interactions[19]. By means of the DMD (1920×1080 pixels with pixel size 10.8 μm × 10.8 μm)-based micro-lithography system and the eighteen-step five-time partly overlapping exposure process[20], the phase pattern in Fig. 1(c) can be accurately transferred onto the SD1-coated LC cell, which is composed of two indium-tin-oxide glass substrates separated by 6 μm spacers. A director-variant LC plate will be naturally formed after E7 is capillarily filled. Figure 1(d) displays the micrograph of the LC CAP with the inset showing the zoom-in image of the central part. The number of rings is doubled compared to Fig. 1(c), which results from the fact that when the LC directors change from 0 to π the bright-to-dark changes twice under the observation with crossed polarizers. The consecutive variation of the brightness also illustrates the continuous orientation of LC directors.

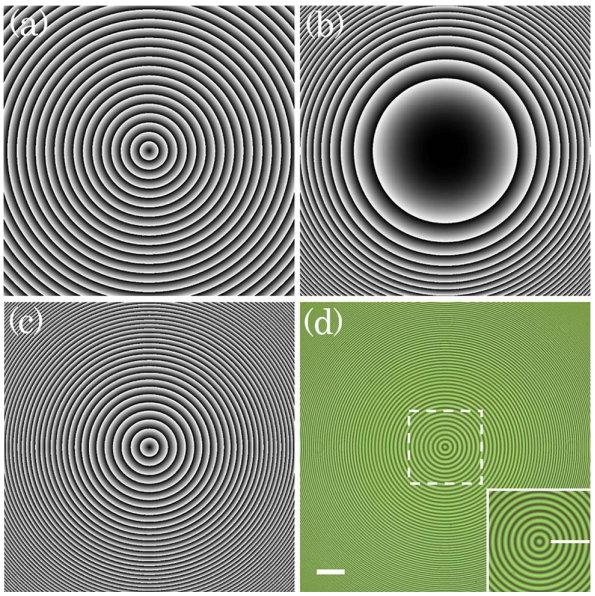

Fig. 1. Patterns of the (a) linear phase, (b) cubic phase, and (c) superimposed phase, where black to white indicates 0 to 2π. (d) Micrograph of the LC CAP with an inset showing the zoom-in image of the central part marked by the dashed lines. The scale bar is 100 μm.

The process of geometric phase modulation can be analyzed by the Jones calculus. The Jones matrix for an optical element with the optical axis orientating as α can be expressed as

$$\mathbf{M} = \cos\frac{\Gamma}{2}\begin{bmatrix} 1 & 0 \\ 0 & 1 \end{bmatrix} - i\sin\frac{\Gamma}{2}\begin{bmatrix} \cos 2\alpha & \sin 2\alpha \\ \sin 2\alpha & -\cos 2\alpha \end{bmatrix}, \tag{2}$$

where $\Gamma = 2\pi\Delta n d/\lambda$ is the phase retardation, Δn is the birefringence of the LC E7 at the incident wavelength λ, and d is the LC cell gap. When the LC CAP is illuminated by a circularly polarized Gaussian beam, i.e., $\mathbf{E}_{\text{in}} = E_0 \times [1, \pm i]^{\text{T}}$, where the sign of the spin eigenstate $+/-$ corresponds to left/right circular polarization (LCP/RCP), the output field can be written as

$$\begin{aligned} \mathbf{E}_{\text{out}} &= \mathbf{M} \cdot \mathbf{E}_{\text{in}} \\ &= E_0 \cos\frac{\Gamma}{2}\begin{bmatrix} 1 \\ \pm i \end{bmatrix} \\ &\quad - E_0 i \sin\frac{\Gamma}{2}\exp\left[\pm i\left(\frac{2\pi r}{d} + \beta r^3\right)\right]\begin{bmatrix} 1 \\ \mp i \end{bmatrix}. \end{aligned} \tag{3}$$

The first term of Eq. (3) is the residual Gaussian beam component, and it can be highly suppressed by electrically tuning the LC CAP to be at half-wave condition. The second term represents the transformed light field based on the geometric phase modulation. It reveals that when the incident polarization is LCP, the radial cubic phase modulation is positive, while the sign of the spin eigenstate changes to be negative, exhibiting an inward-bending or autofocusing CAB with an RCP state. Contrarily, for the RCP incidence, the output state is LCP with a negative modulation, which indicates that the transformed CAB will propagate outward or autodefocus[4]. Therefore, a CAB with polarization-controllable autofocusing or defocusing property will be realized via the photoaligned LC geometric phase plate.

To verify the performance of our sample, we employ an optical setup, as shown in Fig. 2. A Gaussian beam emitted from a He–Ne laser ($\lambda = 632.8$ nm) passes through a polarizer, a quarter-wave plate, and the LC CAP in

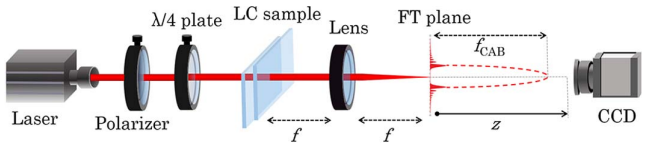

Fig. 2. Optical setup for the generation and modulation of CABs.

sequence. The intensity of the incident light can be adjusted by rotating the polarizer, and the LCP or RCP state can be acquired by setting the angle between the fast axis of the quarter-wave plate and the polarization direction of the polarizer to be 45° or 135°. A lens with focal length $f = 10$ cm is placed at a distance f away from the sample to perform the FT. A CCD is utilized to detect the transformed intensity distribution at different propagation distances. Herein, we define the focal plane of the lens or the FT plane to be the initial observation point $z = 0$.

Figure 3 depicts the propagation dynamics of the generated CAB when the incident polarization is set to be LCP and the voltage at the frequency of 1 kHz applied to the LC CAP is tuned to be 2.49 V to satisfy the half-wave condition. In order to control the light intensity of the CAB at the focus not to exceed the detection range of the CCD, we reduced the power of the input Gaussian laser beam. Due to the brightest ring of the CAB containing almost half of the total energy[4], the sub-rings around the main ring are therefore not so obvious in the inserted transverse intensity patterns, as shown in Fig. 3(a). The situation is similar for the simulated side-view propagation shown in Fig. 3(b) (the intensity distribution is normalized to the peak intensity). However, the detected decrease in the radius R of the main ring and the

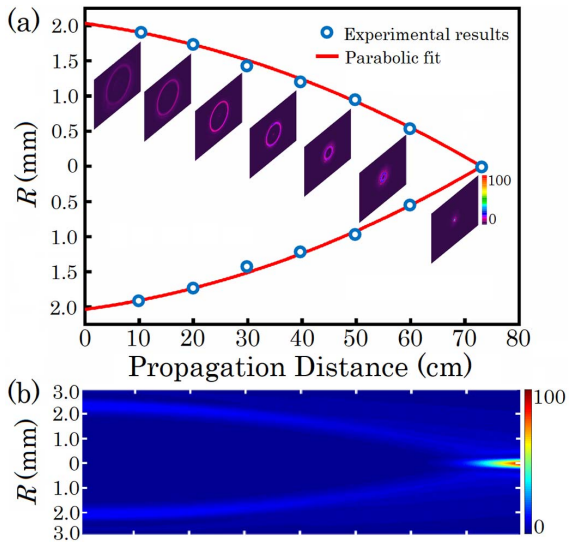

Fig. 3. (a) Experimental and (b) simulated autofocusing dynamics of the CAB. Blue circles in (a) represent the measured radius or the transverse deflection of the CAB, and the red lines are parabolic fit curves. The inserted transverse profiles are detected at $z = 10$, 20, 30, 40, 50, 60, and 74 cm, respectively.

corresponding fitted curves in Fig. 3(a) intuitively illustrate that the CAB accelerates inward and parabolically, leading to the autofocusing behavior of the RCP CAB with an abrupt increase in the peak intensity near the focal point. The measured focal length of the CAB f_{CABM} is 74 cm. The theoretical value can be calculated based on the following expression[10]:

$$f_{\mathrm{CABT}} = \sqrt{\frac{48 f^4 \lambda^2 \beta}{\pi w^3 d}}, \tag{4}$$

where w is the width of the LC CAP. Herein, $w = 1080 \times 1.08\ \mu\mathrm{m} = 1166.4\ \mu\mathrm{m}$ (the size of the phase pattern inserted in the DMD is 1080 pixel × 1080 pixel, and the minification ratio of the DMD system is 10×), $d = 70 \times 1.08\ \mu\mathrm{m} = 75.6\ \mu\mathrm{m}$, and the value of β is 120. Therefore, the theoretical focal length of the CAB f_{CABT} is calculated to be 78 cm. f_{CABM} is pretty consistent with f_{CABT} taking the experimental errors into consideration. Besides, the measured trajectory of the CAB in Fig. 3(a) matches well with the simulated autofocusing propagation dynamics in Fig. 3(b), indicating the robustness of the photoaligned LC geometric phase sample.

Furthermore, the incident polarization is adjusted to RCP to fully investigate the propagation process of the CAB modulated by the LC CAP. Figures 4(a)–4(e) are intensity distributions of the CAB captured at $z = 0$, 20, 40, 60, and 74 cm, respectively. The central Gaussian beam component corresponds to the first term in Eq. (3), which cannot be completely suppressed because of the residual phase of the LC element[21]. However, the maximum efficiency of the generated CAB for both LCP and RCP incidence is ~93%, indicating an efficient geometric phase modulation. It is shown that the radius of the Airy beam becomes larger along with the increase of the propagation distance, which corresponds to the outward propagation dynamics as analyzed above. Also,

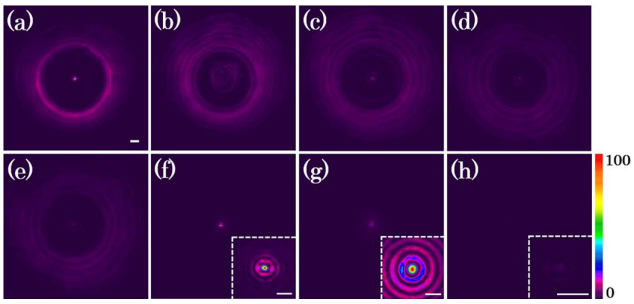

Fig. 4. (a)–(e) Intensity distributions of the defocusing CABs at $z = 0$, 20 40, 60, and 74 cm, (f) autofocusing CAB at $z = 74$ cm by changing the incident polarization from RCP to LCP, and (g) transformed Bessel beam at $z = 90$ cm. The insets in (f) and (g) are the zoom-in images of the central parts. (h) Detected OFF state of the CAB at $z = 74$ cm when the applied voltage is tuned to meet the full-wave condition. The scale bars in (a) and the insets of (f)–(h) indicate 500 μm and 200 μm, respectively.

the average intensity of each Airy ring decreases spontaneously, exhibiting an autodefocusing characteristic. Due to the incident intensity control mentioned above, the detected intensity contrast in Figs. 4(d) and 4(e) is relatively weak. As a contrast, the CAB under LCP's illumination at $z = 74$ cm is also presented in Fig. 4(f), showing a focused intense spot at the axis. Therefore, the switch between the focusing and defocusing states can be easily realized by changing the incident circular polarization. It is worth mentioning that the CAB will morph into a Bessel beam after its focal point[4], which is also verified in Fig. 4(g), detected at $z = 90$ cm. The inset with an increased input power better shows the intensity distribution of the Bessel beam. In addition, a switching ON to OFF state of the CAB can also be achieved by tuning the applied voltage from the half-wave condition (ON state) to the full-wave condition (1 V for the LC CAP or simply over 10 V), as shown in Fig. 4(h). In this case, only the first term in Eq. (3) remains. Therefore, the output field still propagates in the Gaussian beam mode. After the FT plane, the Gaussian beam gradually expands, leading to such a weak intensity at the focal plane of the autofocusing CAB that the light spot can hardly be distinguished even from the zoom-in image in the inset. The comparison between Figs. 4(h) and 4(f) better reveals a quite good OFF state. Moreover, as the focal length of the CAB is dependent on the radius of the initial profile and the acceleration, that is, w, d, and β according to Eq. (4), the focusing dynamics of the LC CAP-mediated CAB is programmable by varying the values of these parameters and choosing proper objective magnification of the DMD-based exposure system[12]. By the way, the adjustment in the focal length of the FT lens f can also affect the focal length of the CAB. In addition, it is worth mentioning that thanks to the excellent rewritability of SD1 and electro-optical tunability of LC materials, the CAP sample is reconfigurable and can be applied for a wide range spectrum[19]. These outstanding qualities provide flexibility for the utilization of the CABs in optical manipulation, light bullets, laser nanosurgery, and so on.

In conclusion, we have demonstrated a practical and convenient way to generate the CABs via a geometric phase element LC CAP. The LC sample is fabricated through the SD1-based photoaligning technique and the DMD-based dynamic photopatterning skill. A characteristic autofocusing process is observed, and the focal distance and propagation dynamics are in accordance with the calculations and simulations. Additionally, the autodefocusing state is also realized by switching the incident circular polarization, exhibiting the advantage of polarization controllability. The switching between ON and OFF states of the CAB can also be achieved by tuning the applied voltage. Besides, the LC CAP sample and the focal length of the CAB can be customized as required. Together with optical reconfigurability and electrical tunability, these merits will promote and expand the applications of CABs in optics and photonics, military field, medical sciences, and even interdisciplinary fields.

This work was supported by the National Natural Science Foundation of China (NSFC) (Nos. 11804277, 11634010, 61675168, and 11774289), the National Key R&D Program of China (No. 2017YFA0303800), the Natural Science Basic Research Plan in Shaanxi Province of China (No. 2019JQ-616), the Open Research Fund of State Key Laboratory of Pulsed Power Laser Technology (No. SKL2019KF08), the Fundamental Research Funds for the Central Universities (Nos. 310201911cx022 and 3102019JC008), the Open Foundation Project of National Laboratory of Solid State Microstructures (No. M31040), and the Anhui Provincial Natural Science Foundation (No. 1908085QF275).

[†]These authors contributed equally to this work.

References

1. G. Siviloglou, J. Broky, A. Dogariu, and D. Christodoulides, Phys. Rev. Lett. **99**, 213901 (2007).
2. N. K. Efremidis and D. N. Christodoulides, Opt. Lett. **35**, 4045 (2010).
3. D. G. Papazoglou, N. K. Efremidis, D. N. Christodoulides, and S. Tzortzakis, Opt. Lett. **36**, 1842 (2011).
4. P. Zhang, J. Prakash, Z. Zhang, M. S. Mills, N. K. Efremidis, D. N. Christodoulides, and Z. Chen, Opt. Lett. **36**, 2883 (2011).
5. P. Panagiotopoulos, D. G. Papazoglou, A. Couairon, and S. Tzortzakis, Nat. Commun. **4**, 2622 (2013).
6. N. K. Efremidis, Z. Chen, M. Segev, and D. N. Christodoulides, Optica **6**, 686 (2019).
7. I. Chremmos, P. Zhang, J. Prakash, N. K. Efremidis, D. N. Christodoulides, and Z. Chen, Opt. Lett. **36**, 3675 (2011).
8. M. Manousidaki, V. Y. Fedorov, D. G. Papazoglou, M. Farsari, and S. Tzortzakis, Opt. Lett. **43**, 1063 (2018).
9. S. Liu, M. Wang, P. Li, P. Zhang, and J. Zhao, Opt. Lett. **38**, 2416 (2013).
10. J. A. Davis, D. M. Cottrell, and D. Sand, Opt. Express **20**, 13302 (2012).
11. Z. Zhang, Z. You, and D. Chu, Light Sci. Appl. **3**, e213 (2014).
12. B. Y. Wei, P. Chen, W. Hu, W. Ji, L. Y. Zheng, S. J. Ge, Y. Ming, V. Chigrinov, and Y. Q. Lu, Sci. Rep. **5**, 17484 (2015).
13. P. Chen, S. J. Ge, W. Duan, B. Y. Wei, G. X. Cui, W. Hu, and Y. Q. Lu, ACS Photon. **4**, 1333 (2017).
14. B. Y. Wei, S. Liu, P. Chen, S. X. Qi, Y. Zhang, W. Hu, Y. Q. Lu, and J. L. Zhao, Appl. Phys. Lett. **112**, 121101 (2018).
15. P. Chen, L. L. Ma, W. Duan, J. Chen, S. J. Ge, Z. H. Zhu, M. J. Tang, R. Xu, W. Gao, T. Li, W. Hu, and Y. Q. Lu, Adv. Mater. **30**, 1705865 (2018).
16. B. Wei, S. Qi, S. Liu, P. Li, Y. Zhang, L. Han, J. Zhong, W. Hu, Y. Lu, and J. Zhao, Opt. Express **27**, 18848 (2019).
17. P. Chen, L. L. Ma, W. Hu, Z. X. Shen, H. K. Bisoyi, S. B. Wu, S. J. Ge, Q. Li, and Y. Q. Lu, Nat. Commun. **10**, 2518 (2019).
18. P. Chen, B. Y. Wei, W. Hu, and Y. Q. Lu, Adv. Mater. **31**, 1903665 (2019).
19. B. Y. Wei, W. Hu, Y. Ming, F. Xu, S. Rubin, J. G. Wang, V. Chigrinov, and Y. Q. Lu, Adv. Mater. **26**, 1590 (2014).
20. P. Chen, B. Y. Wei, W. Ji, S. J. Ge, W. Hu, F. Xu, V. Chigrinov, and Y. Q. Lu, Photon. Res. **3**, 133 (2015).
21. X. W. Lin, W. Hu, X. K. Hu, X. Liang, Y. Chen, H. Q. Cui, G. Zhu, J. N. Li, V. Chigrinov, and Y. Q. Lu, Opt. Lett. **37**, 3627 (2012).